Analytica Chimica Acta 893 (2015) 84–90

Contents lists available at ScienceDirect

Analytica Chimica Acta

journal homepage: www.elsevier.com/locate/aca

Hydrazine selective dual signaling chemodosimetric probe in physiological conditions and its application in live cells

Sandip Nandi [a], Animesh Sahana [a], Sandip Mandal [a], Archya Sengupta [b], Ansuman Chatterjee [b], Damir A. Safin [c, *], Maria G. Babashkina [c], Nikolay A. Tumanov [c], Yaroslav Filinchuk [c], Debasis Das [a, **]

[a] Department of Chemistry, The University of Burdwan, Burdwan, 713104 West Bengal, India
[b] Department of Zoology, Visva Bharati University, Santiniketan, West Bengal, India
[c] Institute of Condensed Matter and Nanosciences, Molecules, Solids and Reactivity (IMCN/MOST), Université catholique de Louvain, Place L. Pasteur 1, 1348 Louvain-la-Neuve, Belgium

HIGHLIGHTS

- A selective rhodamine–cyanobenzene conjugate is synthesized.
- The conjugate is a selective dual signaling chemodosimetric probe towards hydrazine.
- Spirolactam ring opening of the probe, followed by its hydrolysis, is the sensing mechanism.
- The probe detects hydrazine in the human breast cancer cells MCF-7 imaging.

GRAPHICAL ABSTRACT

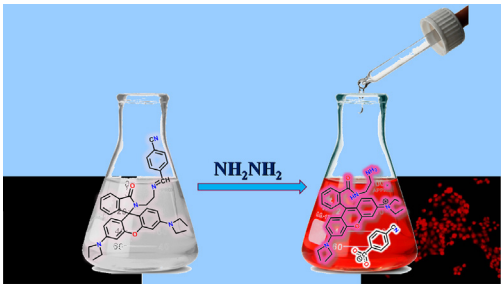

ARTICLE INFO

Article history:
Received 31 May 2015
Received in revised form
16 August 2015
Accepted 24 August 2015
Available online 1 September 2015

Keywords:
Chemodosimetric probe
Hydrazine
Rhodamine
"Turn-on" fluorescence
Cell imaging

ABSTRACT

A rhodamine–cyanobenzene conjugate, (*E*)-4-((2-(3′,6′-bis(diethylamino)-3-oxospiro[isoindoline-1,9′-xanthene]-2-yl)ethylimino)methyl)benzonitrile (**1**), which structure has been elucidated by single crystal X-ray diffraction, was synthesized for selective fluorescent "turn-on" and colorimetric recognition of hydrazine at physiological pH 7.4. It was established that **1** detects hydrazine up to 58 nM. The probe is useful for the detection of intracellular hydrazine in the human breast cancer cells MCF-7 using a fluorescence microscope. Spirolactam ring opening of **1**, followed by its hydrolysis, was established as a probable mechanism for the selective sensing of hydrazine.

1. Introduction

Hydrazine (N_2H_4), a simple diamine and powerful reducing agent, has been used as a fuel and propellant in aircraft due to its flammable and detonable characteristics [1]. Hydrazine is widely used in many chemical, pharmaceutical and agricultural industries involving catalysts, metal anticorrosion, textile dyes and

* Corresponding author.
** Corresponding author.
E-mail addresses: damir.a.safin@gmail.com (D.A. Safin), ddas100in@yahoo.com (D. Das).

http://dx.doi.org/10.1016/j.aca.2015.08.041
0003-2670/

pharmaceutical intermediates [2–4]. In contrast to its usefulness, toxic and carcinogenic effect of hydrazine potentially lead to serious environmental pollution during its production, purification, utilization and transportation [5,6]. It has been reported that hydrazine is a neurotoxin and has severe mutagenic effects causing infections of the respiratory tract and damage to the lungs, liver, kidneys and central nervous system [7–9]. Furthermore, hydrazine produces toxicity by interfering with a number of metabolic processes such as gluconeogenesis and glutamine syntheses [10]. Although there is no endogenous hydrazine in live cells, it is readily absorbed by oral, dermal or inhalation routes of exposure, being harmful to live cells. Thus, it is important to develop selective, sensitive and easy methods for the detection of hydrazine under biocompatible conditions at physiological pH [11]. Hydrazine can be routinely analyzed by some traditional method such as electrochemical analysis [12] and chromatography [13], including gas chromatography [14] and HPLC [15]. However, these techniques are often time consuming, require complicated sample processing and destructive for tissues or cells. Therefore considerable efforts have been made to synthesize probes that can detect hydrazine in a selective and sensitive manner. Probes based on changes in fluorescence induced by analytes are particularly attractive because of the simplicity of their utilization and lower detection limits [16,17]. Recently, few fluorescent probes, based on the coumarin [18–20], fluorescein [21] as well as other fluorophores [22–28], have been developed for the hydrazine detection. However, most of these reported fluorescent probes worked in pure organic solvents, that impeded their application for the hydrazine detection in living cells at physiological pH. Pronounced spectroscopic properties of rhodamine B, such as visible light excitation as well as long wavelength emission and high fluorescence quantum yield, make it a good choice for the designing of fluorescence probes [29]. Large fluorescence enhancement as well as colorimetric change with absorption at around 550 nm is due to spirolactam ring opening [30]. Careful observation of number of rhodamine based probes reported in the literature indicates that their sensing properties mostly depend on the appended functionality but not only on the rhodamine unit alone. This fact inspired us to design and synthesize a new rhodamine B based chemodosimetric probe (*E*)-4-((2-(3′,6′-bis(diethylamino)-3-oxospiro[isoindoline-1,9′-xanthene]-2-yl)ethylimino)methyl)benzonitrile (**1**) having an electron withdrawing nitrile group at the *para*-position of the appended unit. Moreover, the probe **1** is also useful for intra-cellular hydrazine imaging and quantitative determination at physiological conditions. Another reference compound (*E*)-3′,6′-bis(diethylamino)-2-(2-(4-(dimethylamino)benzylideneamino)ethyl)spiro[isoindoline-1,9′-xanthen]-3-one (**2**) is also synthesized and studied to further strengthen the proposed sensing mechanism.

2. Experimental

2.1. Materials and methods

Rhodamine B, 4-cyanobenzaldehyde, 4-(dimethylamino)benzaldehyde and high-purity HEPES were purchased from Sigma Aldrich (India). Spectroscopic grade solvents have been used. Other chemicals were of analytical reagent grade and used without further purification. Mili-Q 18.2 MΩ cm^{-1} water has been used throughout all the experiments. A Shimadzu Multi Spec 1501 UV–vis spectrophotometer was used for recording absorption spectra. ^1H NMR titration in CD_3CN was recorded using a Bruker Avance 500 (500 MHz). Steady-state fluorescence experiments were performed using a Hitachi F-4500 spectrofluorimeter. The electrospray ionization (ESI^+) mass spectra were measured with a Finnigan-Mat TCQ 700 mass spectrometer. pH measurements were performed with a Systronics digital pH meter (model 335). Elemental analyses were performed on a Perkin Elmer 2400 CHN analyzer.

2.2. In vitro cell imaging

Human breast cancer cell line MCF-7 was grown in DMEM (Sigma, St. Louis, USA) supplemented with 10% fetal bovine serum (Sigma, St. Louis, USA), 2 mM glutamine, 100 U m/L penicillin-streptomycin solution (Gibco, Invitrogen, USA) in the presence of 5% CO_2 at 37 °C. For *in vitro* imaging studies, cells were seeded in 6 well culture plates with a seeding density of 10^5 cells per well. After reaching 60–70% confluence, the previous media was replaced with serum free media, supplemented by hydrazine and **1** at 50 μM and 20 μM, respectively, and incubated for 2 h to facilitate hydrazine or **1** uptake by cells. Then cells were placed under an inverted microscope (Dewinter, Italy) at different magnifications to examine any adverse effect on cellular morphology. **1** treated cells were then incubated with hydrazine for 15–30 min and observed under an inverted fluorescence microscope at different magnifications with a blue filter. Images were taken through an attached ccd camera with help of the Bio-Wizard 4.2 software. A control experiment was done using medium devoid of hydrazine.

2.3. Cytotoxicity assay

In vitro cytotoxicity was measured using the colorimetric methyl thiazolyl tetrazolium (MTT) assay on the mouse bone marrow cells [31–33]. Cells were seeded into the 24-well tissue culture plate in the presence of 500 μL Dulbecco's modifed eagle medium (DMEM) supplemented with 10% fetal bovine serum (FBS) and 1% penicillin/streptomycin at 37 °C and 5% CO_2 atmosphere for overnight and then incubated for 6 h in the presence of **1** at different concentrations (10, 20 and 40 μM). Then cells were washed with PBS buffer and 500 μL supplemented DMEM medium was added. Subsequently, 50 μL MTT (5 mg/mL) was added to each well and incubated for 4 h. Violet formazan was dissolved in 500 μL sodium dodecyl sulfate solution in the water-DMF mixture. Absorbance of the solution was measured at 558 nm using a microplate reader. The cell viability was determined by assuming 100% cell viability for cells without **1**.

2.4. UV–vis and fluorescence titration

The path length of cells used for the absorption and emission studies was 1 cm. For UV–vis and fluorescence titrations, a stock solution of **1** (10 μM) was prepared in the HEPES (0.1 M) buffered CH_3CN–H_2O (9:1, v/v) solution at pH 7.4. Working solutions of **1** and hydrazine were prepared from their respective stock solutions.

2.5. Quantum yield measurements

The fluorescence quantum yields were determined using Rhodamine B as a reference with a known ϕ_{ref} value of 0.65 in basic EtOH [34]. The area of the emission spectrum was integrated using the software available in the instrument and the quantum yield was calculated according to the following equation [35]: $\phi_{sample} = \phi_{ref} \times [A_{sample}/A_{ref}] \times [OD_{ref}/OD_{sample}] \times [(\eta_{sample})^2/(\eta_{ref})^2]$, where ϕ_{sample} and ϕ_{ref} are the fluorescence quantum yield of the sample and reference, respectively; A_{sample} and A_{ref} are the area under the fluorescence spectra of the sample and the reference, respectively; OD_{sample} and OD_{ref} are the corresponding optical densities of the sample and the reference solution at the wavelength of excitation; η_{sample} and η_{ref} are the refractive index of the sample and reference, respectively.

2.6. Synthesis of **1** and **2**

4-Cyanobenzaldehyde or 4-(dimethylamino)benzaldehyde (0.270 and 0.307 g, respectively; 2.06 mmol) was added to a solution of 2-(2-aminoethyl)-3′,6′-bis(diethylamino)spiro[isoindoline-1,9′-xanthen]-3-one (1.0 g, 2.06 mmol) in dry EtOH (30 mL). The mixture was refluxed for 12 h. Then the solvent was removed in vacuum and the crude product was purified by recrystallization from CH_3CN.

1. Yield: 1.096 g (89%). ESI^+, *m/z* (*I*%): 620.78 (100) $[M+Na]^+$. *Anal*. Calc. for $C_{38}H_{39}N_5O_2$ (597.76) (%): C 76.35, H 6.58 and N 11.72; found: C 76.21, H 6.64 and N 11.59.

2. Yield: 1.066 g (84%). ESI^+, *m/z* (*I*%): 638.85 (100) $[M+Na]^+$. *Anal*. Calc. for $C_{39}H_{45}N_5O_2$ (615.82) (%): C 76.07, H 7.37 and N 11.37; found: C 75.95, H 7.46 and N 11.28.

2.7. Crystal structure determination

The structure of **1** was solved from single-crystal synchrotron X-ray diffraction data, which were collected at the Swiss-Norwegian Beam Line BM01A at the European Synchrotron Radiation Facility (ESRF) (Grenoble, France), using a PILATUS 2M hybrid pixel detector, at a wavelength of 0.6984 Å, and a sample-to-detector distance of 144 mm. The collection mode was φ-scans at 296(2) K. The data were converted and integrated using the SNBL toolbox software [36] and CrysAlisPro software [37]. Crystal diffracted up to 1.04 Å resolution. The multi-scan absorption correction procedure implemented in the CrysAlisPro software was applied. Crystal was twinned, and the hkl5 file was generated using Platon [38]. The structure was solved by MDM procedure using the SIR2014 [39] program and refined by full-matrix least squares on $|F|^2$ using SHELXL-2014 [40] and the shelXLe shell [41]. Non-hydrogen atoms were refined anisotropically and hydrogen atoms were placed on calculated positions in riding mode with temperature factors fixed at 1.2 times U_{eq} of the parent atoms and 1.5 times U_{eq} for methyl groups. Disorder of two ethyl groups was modeled. Rigid group restrains were applied to some benzene rings. Also few constrains to distances and temperature factors were applied. Figures were generated using the program Mercury [42]. $C_{38}H_{39}N_5O_2$, $M_r = 597.74$ g mol^{-1}, monoclinic, space group $P2_1/c$, $a = 44.262(5)$, $b = 16.3484(10)$, $c = 9.0562(8)$ Å, $\beta = 102.351(10)^\circ$, $V = 6401.5(10)$ Å^3, $Z = 8$, $\rho = 1.240$ g cm^{-3}, 6486 unique reflections, R_1(all) = 0.1673, $R_1[F^2 > 2\sigma F^2] = 0.1046$, wR_2(all) = 0.2890.

CCDC 995593 contains the supplementary crystallographic data. These data can be obtained free of charge via http://www.ccdc.cam.ac.uk/conts/retrieving.html, or from the Cambridge Crystallographic Data Centre, 12 Union Road, Cambridge CB2 1EZ, UK; fax: (+44) 1223 336 033; or e-mail: deposit@ccdc.cam.ac.uk.

3. Results and discussion

Compound **1** was readily obtained by reacting 2-(2-aminoethyl)-3′,6′-bis(diethylamino)spiro[isoindoline-1,9′-xanthen]-3-one with 4-formylbenzonitrile (Scheme 1).

The formation of **1** was supported by the ^{1}H NMR spectroscopy data (Fig. S1 in the Supplementary data) and ESI^+ mass spectrometry, while its crystal structure was elucidated from single crystal X-ray diffraction (Fig. 1, Table S1 in the Supplementary data).

Although the probe is selective towards hydrazine in pure aqueous medium, however, the sensitivity is less due to its relatively higher emission intensity compared to the CH_3CN–water (9:1, v/v) medium. This allowed us to monitor the sensing properties in the latter mixture. It was found that **1** exhibits very weak fluorescence at the pH range 2–10, indicating its stability in a wide pH range (Fig. S2 in the Supplementary data). It is most likely that the presence of the electron withdrawing nitrile group influences on the spirolactam ring of rhodamine to make it less reactive to open at low pH. Higher fluorescence enhancement of the probe at lower pH is also explicable. At low pH, hydrazine ($pK_a = 8.1$) remains in a mono protonated form, which is more active to form a proposed hydrogen bonding interaction with the probe. However, pH 7.4 was chosen as working pH because of its biological importance. Upon treatment with hydrazine, the emission intensity of **1** increases at physiological pH 7.4 too. Thus, the probe **1** was found to be promising for biological applications and all further studies were performed in the HEPES (0.1 M) buffered CH_3CN–H_2O (9:1, v/v) solution at pH 7.4 and at room temperature.

Upon excitation at 500 nm **1** shows poor quantum yield of 0.02, indicating that the spirolactum ring of the rhodamine fragment was closed in the working solution. However, treatment with hydrazine immediately elicited a dramatic “turn-on” fluorescence response at 570 nm with about 25 times increase in the fluorescence quantum yield (0.49). The intensity of the emission spectra at 570 nm gradually increased upon incremental addition of hydrazine up to 300 μM whereupon the red color, observed under UV light, intensified (Fig. 2).

A 55 fold increase of absorbance at 543 nm, accompanied with the saturation of pink color was observed upon addition of 30 equivalents hydrazine, indicating spirolactum ring opening (Fig. 3).

A sigmoidal curve was obtained when emission intensities of **1** (10 μM) were plotted as a function of externally added hydrazine, exhibiting a linear region up to 150 μM hydrazine (Fig. 4), allowing determination of the unknown concentration of hydrazine. The plot of absorbance at 543 nm of **1** (10 μM) as a function of externally added hydrazine might also be useful for the same purpose (Fig. S3 in the Supplementary data).

Job's plot indicated a 1:1 stoichiometry of the [**1**-hydrazine] system (Fig. 5). The detection limit (DL) of **1** towards hydrazine was determined using the equation [43]: DL = K × Sb1/S, where K = 2 or 3 (we took 3 in this case), Sb1 was the standard deviation of the blank solution, S was the slope of the calibration curve. The value of DL was found to be 58 nM. These results demonstrated that **1** might be useful for both qualitative and quantitative determination of hydrazine at the nanomolar level.

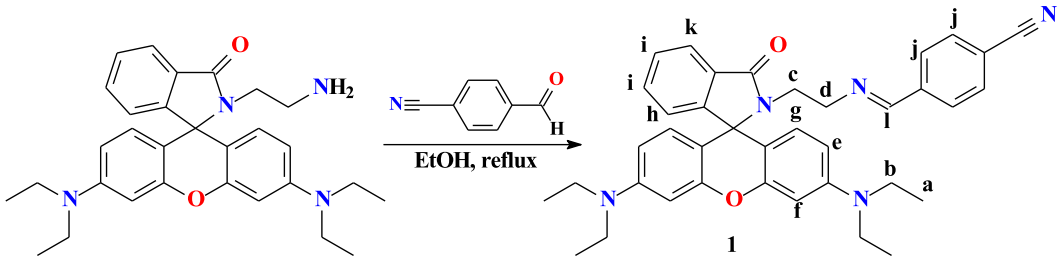

Scheme 1. Preparation of **1**.

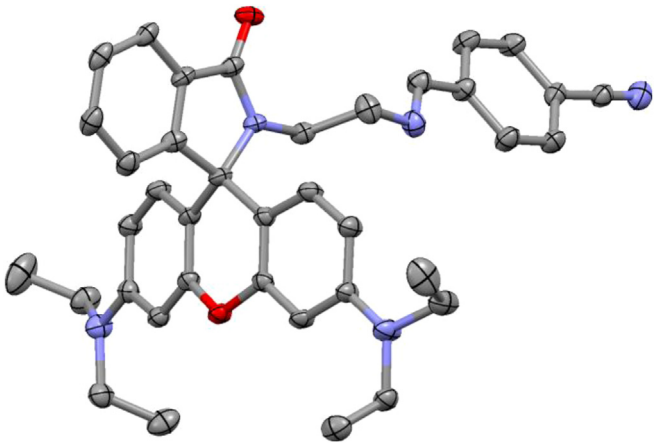

Fig. 1. Single crystal X-ray structure of **1** (hydrogen atoms were omitted).

To shed some light on the proposed interaction of **1** with hydrazine, ^{1}H NMR titration was performed by concomitant addition of hydrazine to the CD_3CN solution of **1** (Fig. S1 in the Supplementary data). ^{1}H NMR titration shows drastic changes of the spectra of **1** upon gradual addition of hydrazine (Fig. S1 in the Supplementary data). A new broad singlet at 6.36 ppm, corresponding to the NH proton generated due to spirolactam ring opening, and disappearance of the CH=N proton (marked as "l" in Scheme 1) due to hydrolysis of the imine bond, were clearly observed. Ethylene protons (marked as "c" and "d" in Scheme 1) appeared as two separate triplets at 2.38 and 3.15 ppm, while a single broad triplet at 3.52 ppm for the same protons was observed in the ^{1}H NMR spectrum of free **1** (Fig. S1 in the Supplementary data). Furthermore, two significantly overlapped singlets (marked as "j" in Scheme 1) at about 7.82 ppm, corresponding to the 4-cyanophenylene fragment, in the spectrum of the probe were now changed to a multiplet at 7.57–7.74 ppm. With all this in mind,

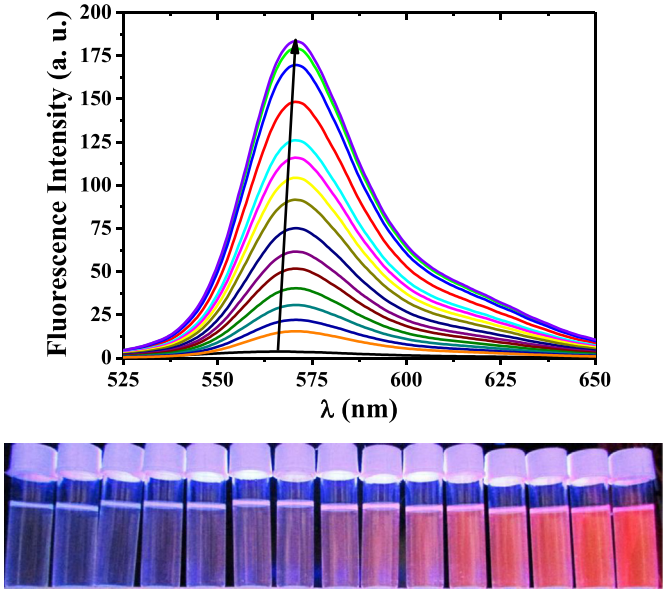

Fig. 2. Changes of the emission spectra at λ_{ex} = 500 nm (top) and UV light irradiated fluorescence color changes (bottom) of the solution of **1** (10 μM, CH_3CN–H_2O (9:1, v/v), 0.1 M HEPES buffer, pH 7.4) upon externally added hydrazine (0.01, 0.1, 1, 5, 10, 25, 50, 75, 100, 125, 150, 175, 200, 250 and 300 μM). (For interpretation of the references to colour in this figure legend, the reader is referred to the web version of this article.)

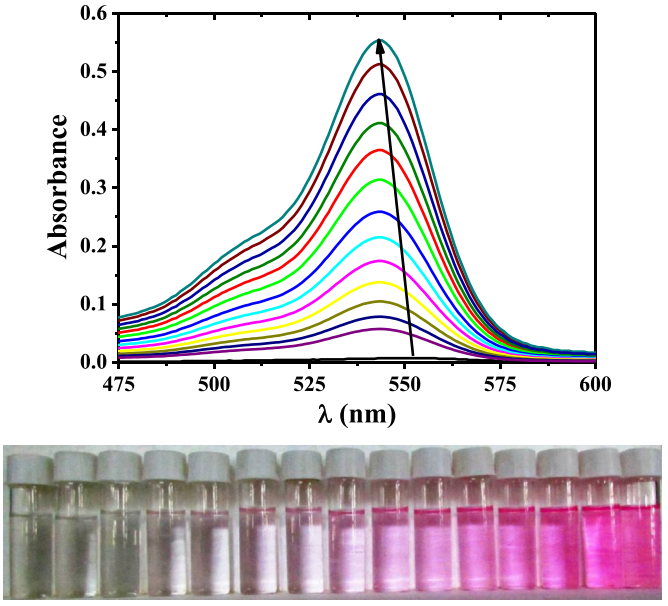

Fig. 3. Changes of the UV–vis spectra (top) and naked eye color changes (bottom) of the solution of **1** (10 μM, CH_3CN–H_2O (9:1, v/v), 0.1 M HEPES buffer, pH 7.4) upon externally added hydrazine (0.01, 0.1, 1, 5, 10, 25, 50, 75, 100, 125, 150, 175, 200, 250 and 300 μM). (For interpretation of the references to colour in this figure legend, the reader is referred to the web version of this article.)

the probable sensing mechanism for hydrazine by **1** was portrayed (Scheme 2). Hydrazine, most likely, forms a hydrogen bonded dimer with the probe **1**, yielding an electron deficient imine carbon. As a result, the latter atom can be "attacked" by the oxygen atom of the water/hydroxyl molecule, thus, resulting in the hydrolysis of **1** accompanied with a spirolactam ring opening (Scheme 2). This assumption was also corroborated from comparison of the ESI$^+$ mass spectra of free **1** and its mixture with five equivalents of hydrazine (Fig. S4 in the Supplementary data). In particular, the presence of the characteristic peaks for the resulting cationic compound at m/z = 485.71 (I = 100%) and 4-cyanobenzoic acid ($[M+Na+H]^+$ = 170.14, I = 26%) supported the mechanism.

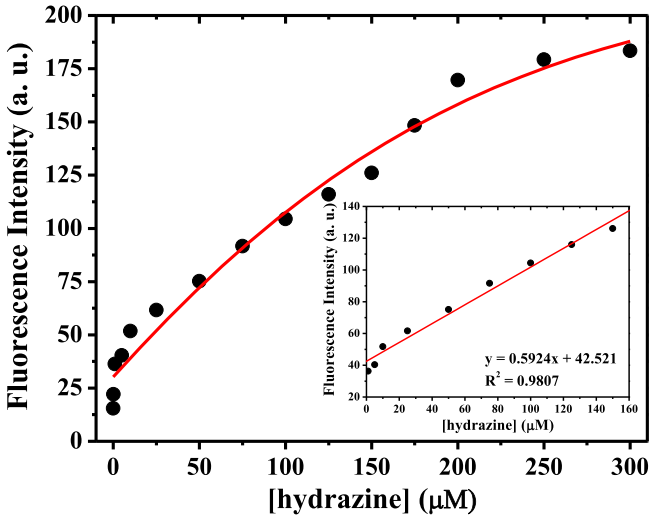

Fig. 4. Plot of the fluorescence intensity of **1** (10 μM, CH_3CN–H_2O (9:1, v/v), 0.1 M HEPES buffer, pH 7.4, λ_{ex} = 500 nm, λ_{em} = 570 nm) as a function of externally added hydrazine (0.01, 0.1, 1, 5, 10, 25, 50, 75, 100, 125, 150, 175, 200, 250 and 300 μM). Inset shows the linearity of the plot from 1.0 to 150.0 μM of added hydrazine.

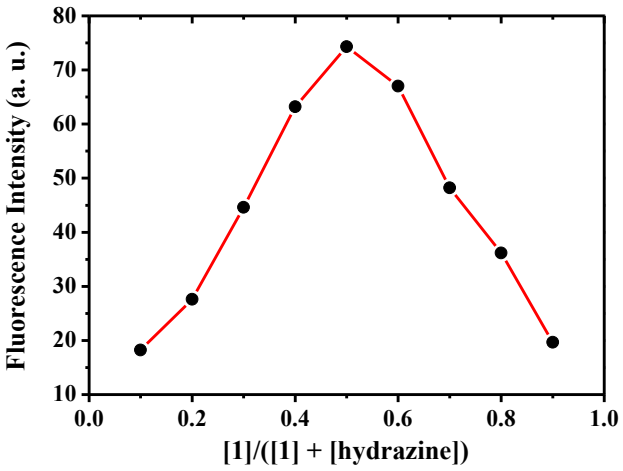

Fig. 5. Job's plot for the determination of stoichiometry of the [**1**-hydrazine] system (λ_{ex} = 500 nm, λ_{em} = 570 nm).

Moreover, the reference compound **2** (Scheme S1 and Fig. S5 in the Supplementary data), where the −CN group is replaced by the $-NMe_2$ group, showed neither colorimetric nor fluorometric (Fig. S6 in the Supplementary data) responses in the presence of hydrazine revealing its unreactive nature towards hydrazine. Thus, the −CN group in **1** plays a crucial role for hydrazine assisted hydrolysis of the imine bond of the probe.

Selectivity of **1** towards hydrazine in the presence of environmentally as well as biologically important ions such as F^-, Cl^-, Br^-, I^-, HS^-, CN^-, ClO_4^-, $H_2PO_4^-$, NO_3^-, SO_4^{2-}, $H_2AsO_4^-$, Li^+, Na^+, K^+, Ca^{2+}, Mg^{2+}, Co^{2+}, Cu^{2+}, Zn^{2+}, Cd^{2+}, Pb^{2+}, Ni^{2+}, Hg^{2+}, Cr^{3+} and Fe^{3+} was also examined. No significant changes in emission (Fig. S7 in the Supplementary data) and absorbance spectra were observed (Fig. S8 in the Supplementary data). Furthermore, only an insignificant change was observed upon the addition of ammonium hydroxide (NH_4OH), ethylenediamine ($(NH_2CH_2)_2$), dimethylamine (Me_2NH), triethylamine (Et_3N), hydroxylamine (NH_2OH), pyridine (Py), aniline ($C_6H_5NH_2$), diethylenetriamine ($NH(CH_2CH_2NH_2)_2$) and cysteine (Cys) to the solution of **1** with hydrazine (Figs. S7 and S8 in the Supplementary data). No other analytes interfere during the fluorometric detection of hydrazine by the probe (Fig. 6). These results approved the remarkably higher selectivity of **1** towards hydrazine over other competitive ions at physiological pH 7.4.

It was also established that paper strips, soaked with **1**, can be efficiently used for visible detection of hydrazine (Fig. 7).

To examine the utility of the probe **1** in biological systems, it was applied to the human breast cancer cells MCF-7. Cells remained non-fluorescent when treated either with hydrazine or **1** but exhibited strong red color fluorescence after addition of hydrazine to the cells incubated with **1** (Fig. 8). Fluorescence imaging also indicates that **1** stain living cells without any harm (cells remained alive even after several hours of exposure to 20 μM of **1**), making it useful to monitor the hydrazine accumulation in biological systems. We have also performed the MTT assay of **1** to check the cell viability at the condition of *in vitro* cell imaging (Fig. 9). The results indicate that a significant number of cells are alive up to 6 h.

Moreover, the probe **1** is successfully used for the quantitative determination of intra-cellular hydrazine. The human breast cancer cells MCF-7 were incubated with four different concentrations of hydrazine (20, 40, 80 and 160 μM) (Fig. S9 in the Supplementary data). Fluorescence images, recorded by a fluorescence microscope at λ_{ex} = 500 nm, were recorded using the same exposure time of 50 ms. Corrected total cell fluorescence (CTCF) was calculated using the following equations [44]: CTCF = Integrated Density - – (Area of a selected cell × Mean fluorescence of background readings). All measurements were performed using the ImageJ software [45]. The CTCF values of the four samples were then plotted *vs.* the corresponding hydrazine concentration (Fig. S9 in the Supplementary data). From the fluorescence image of the human breast cancer cells MCF-7 after 2 h incubation with **1** (20 μM) followed by the addition of hydrazine (50 μM) (Fig. 8C), the CTCF

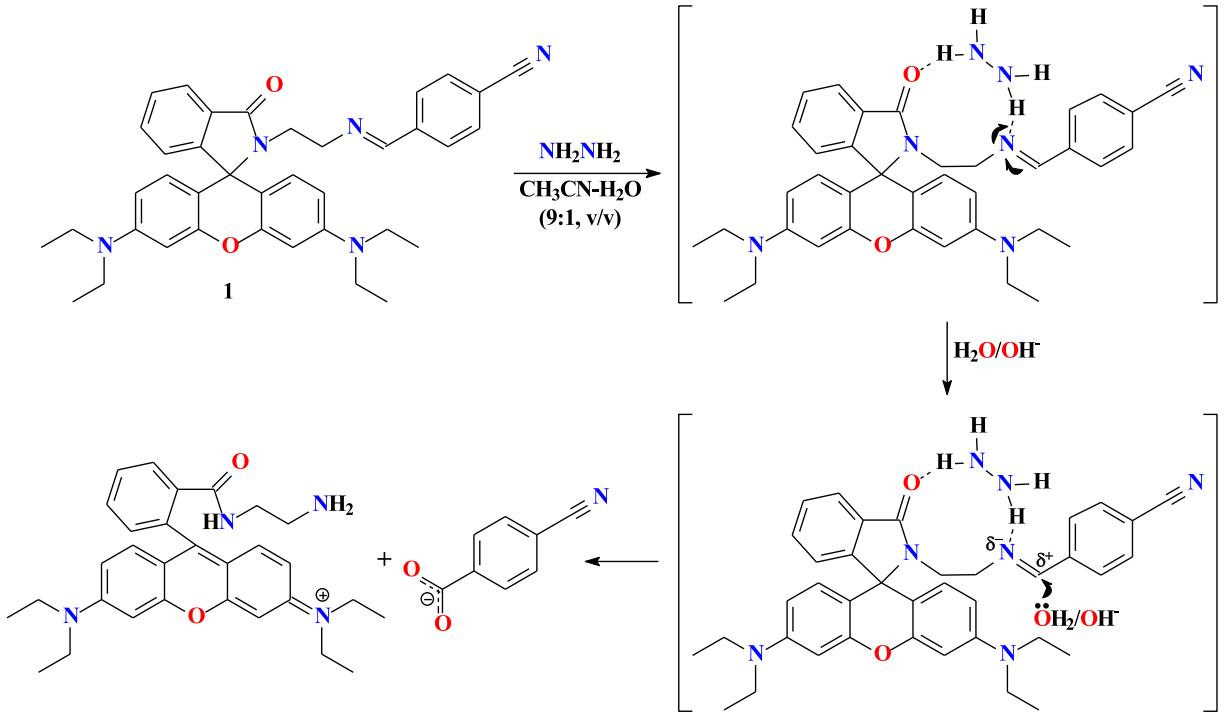

Scheme 2. Probable sensing mechanism of hydrazine by **1**.

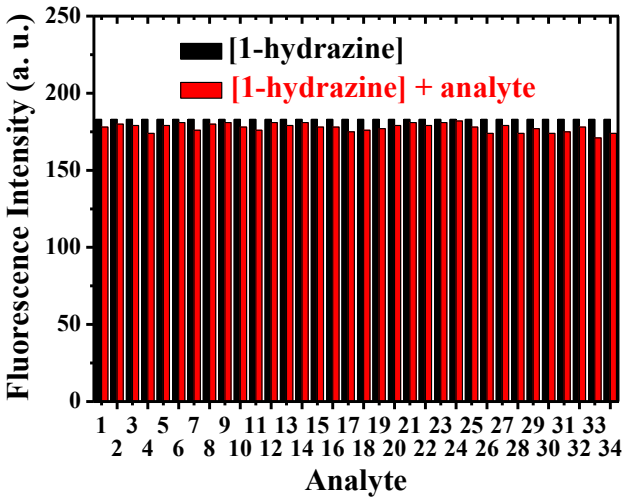

Fig. 6. Interference of different analytes (300 μM; F^- (1), Cl^- (2), Br^- (3), I^- (4), HS^- (5), CN^- (6), ClO_4^- (7), $H_2PO_4^-$ (8), NO_3^- (9), SO_4^{2-} (10), $H_2AsO_4^-$ (11), Li^+ (12), Na^+ (13), K^+ (14), Ca^{2+} (15), Mg^{2+} (16), Co^{2+} (17), Cu^{2+} (18), Zn^{2+} (19), Cd^{2+} (20), Pb^{2+} (21), Ni^{2+} (22), Hg^{2+} (23), Cr^{3+} (24), (25), NH_4OH (26), $(NH_2CH_2)_2$ (27), Me_2NH (28), Et_3N (29), NH_2OH (30), Py (31), $C_6H_5NH_2$ (32), $NH(CH_2CH_2NH_2)_2$ (33), Cys (34)) on the determination of hydrazine by **1** (10 μM, CH_3CN–H_2O (9:1, v/v), 0.1 M HEPES buffer, pH 7.4, λ_{ex} = 500 nm, λ_{em} = 570 nm).

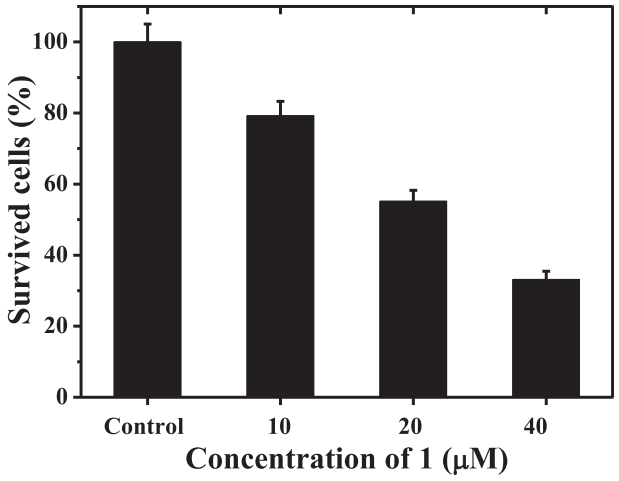

Fig. 9. Survival ability of mouse bone marrow cells after treatment with different concentration of **1** after 6 h. The value of IC_{50} is 24.6 μM.

characterized cyanophenyl appended rhodamine ethylene derivative. Instant visual detection of hydrazine was also demonstrated with a paper strip soaked with the probe. Intracellular imaging and

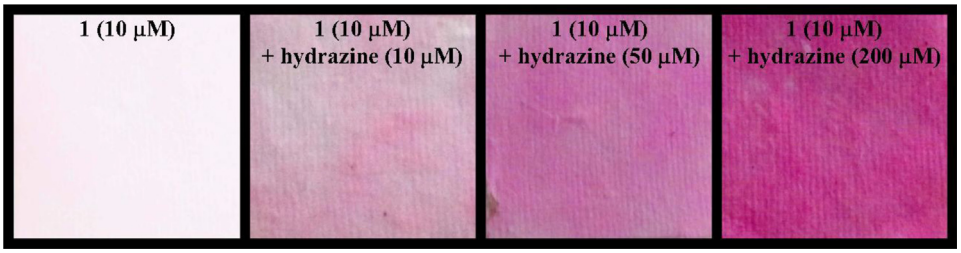

Fig. 7. Photographs of paper strips, taken at ambient light, soaked in the solution of **1** (10 μM, CH_3CN–H_2O (9:1, v/v), 0.1 M HEPES buffer, pH 7.4) followed by addition of different amounts of hydrazine.

Fig. 8. Fluorescence images, recorded by a fluorescence microscope at λ_{ex} = 500 nm, of the human breast cancer cells MCF-7 after 2 h incubation with hydrazine (50 μM) (A), **1** (20 μM) (B) and **1** (20 μM) followed by the addition of hydrazine (50 μM) (C).

value was calculated, using the above equation and the ImageJ software, and found as 151326. Using the calibration plot (Fig. S9 in the Supplementary data), the intracellular hydrazine concentration was found to be 47.6 μM. This value is very close to the concentration of hydrazine (50 μM), the cells are actually treated with (Fig. 8C). Thus, using this developed technique, an unknown intracellular hydrazine concentration can be determined.

4. Conclusions

In summary, fluorescence and colorimetric detection of hydrazine at a nanomolar level was achieved with the X-ray structurally quantitative determination of hydrazine in the human breast cancer cells (MCF-7) was achieved successfully.

Acknowledgment

S. Nandi, S. Mondal and A. Sahana are grateful to UGC and CSIR, New Delhi for fellowships. We are grateful to DST (Gov. of WB) and FNRS (Belgium) for funding. We thank WBI (Belgium) for the postdoctoral positions allocated to D. A. Safin and M. G. Babashkina and Fonds Spéciaux de Recherche (UCL) for the incoming postdoctoral fellowship co-funded by the Marie Curie actions of the European Commission granted to N. A. Tumanov.

Appendix A. Supplementary data

Supplementary data related to this article can be found at http://dx.doi.org/10.1016/j.aca.2015.08.041.

References

[1] S.D. Zelnick, D.R. Mattie, P.C. Stepaniak, Occupational exposure to hydrazines: treatment of acute central nervous system toxicity, Aviat. Space Environ. Med. 74 (2003) 1285–1291.
[2] S.S. Narayanan, F. Scholz, A comparative study of the electrocatalytic activities of some metal hexacyanoferrates for the oxidation of hydrazine, Electroanalysis 11 (1999) 465–469.
[3] U. Ragnarsson, Synthetic methodology for alkyl substituted hydrazines, Chem. Soc. Rev. 30 (2001) 205–213.
[4] J.I. Kroschwitz, A. Seidel, Hydrazine and its Derivatives in Kirk-Othmer Encyclopedia of Chemical Technology, fifth ed., vol. 13, Wiley, NewYork, 2005, pp. 562–607.
[5] W.C. Keller, Toxicity assessment of hydrazine fuels, Aviat. Space Environ. Med. 59 (1988) A100–A106.
[6] S. Budavari (Ed.), The Merck Index, twelfth ed., Merck Research Laboratories, Whitehouse Station, NJ, 1996, p. 816.
[7] Y.Y. Liu, I. Schmeltz, D. Hoffman, Chemical studies on tobacco smoke. XXVII. Quantitative analysis of hydrazine in tobacco and cigarette smoke, Anal. Chem. 46 (1974) 885–889.
[8] C.A. Reilly, S.D. Aust, Peroxidase substrates stimulate the oxidation of hydralazine to metabolites which cause single-strand breaks in DNA, Chem. Res. Toxicol. 10 (1997) 328–334.
[9] S. Garrod, M.E. Bollard, A.W. Nicholls, S.C. Connor, J. Connelly, J.K. Nicholson, E. Holmes, Integrated metabonomic analysis of the multiorgan effects of hydrazine toxicity in the rat, Chem. Res. Toxicol. 18 (2005) 115–122.
[10] J. Kleineke, H. Peters, H.D. Soling, Inhibition of hepatic gluconeogenesis by phenethylhydrazine (phenelzine), Biochem. Pharmacol. 28 (1979) 1379–1389.
[11] Z. Xu, S.J. Han, C. Lee, J. Yoon, D.R. Spring, Development of off-on fluorescent probes for heavy and transition metal ions, Chem. Commun. 46 (2010) 1679–1681.
[12] C.B. McAuley, C.E. Banks, A.O. Simm, T.G.J. Jones, R.G. Compton, The electroanalytical detection of hydrazine: a comparison of the use of palladium nanoparticles supported on boron-doped diamond and palladium plated BDD microdisc array, Analyst 131 (2006) 106–110.
[13] D.P. Elder, D. Snodin, A.J. Teasdale, Control and analysis of hydrazine, hydrazides and hydrazones–genotoxic impurities in active pharmaceutical ingredients (APIs) and drug products, Pharm. Biomed. Anal. 554 (2011) 900–910.
[14] M. Sun, L. Bai, D.Q. Lui, A generic approach for the determination of trace hydrazine in drug substances using in situ derivatization-headspace GC-MS, J. Pharm. Biomed. Anal. 49 (2009) 529–533.
[15] H. Bhutani, S. Singh, S. Vir, K.K. Bhutani, R. Kumar, A.K. Chakraborti, K.C. Jindal, LC and LC-MS study of stress decomposition behaviour of isoniazid and establishment of validated stability-indicating assay method, J. Pharm. Biomed. Anal. 43 (2007) 1213–1220.
[16] R. Martínez-Mañez, F. Sancenon, Fluorogenic and chromogenic chemosensors and reagents for anions, Chem. Rev. 103 (2003) 4419–4476.
[17] S.A. El-Safty, M.A. Shenashen, Mercury-ion optical sensors, Trends Anal. Chem. 38 (2012) 98–115.
[18] M.G. Choi, J. Hwang, J.O. Moon, J. Sung, S.K. Chang, Hydrazine-selective chromogenic and fluorogenic probe based on levulinated coumarin, Org. Lett. 13 (2011) 5260–5263.
[19] J. Fan, W. Sun, M. Hu, J. Cao, G. Cheng, H. Dong, K. Song, Y. Liu, S. Sun, X. Peng, An ICT-based ratiometric probe for hydrazine and its application in live cells, Chem. Commun. 48 (2012) 8117–8119.
[20] S. Goswami, S. Das, K. Aich, D. Sarkar, T.K. Mondal, A coumarin based chemodosimetric probe for ratiometric detection of hydrazine, Tetrahedron Lett. 55 (2014) 2695–2699.
[21] M.G. Choi, J.O. Moon, J. Bae, J.W. Lee, S.K. Chang, Dual signaling of hydrazine by selective deprotection of dichlorofluorescein and resorufin acetates, Org. Biomol. Chem. 11 (2013) 2961–2965.
[22] X. Chen, Y. Xiang, Z. Li, A. Tong, Sensitive and selective fluorescence determination of trace hydrazine in aqueous solution utilizing 5-chlorosalicylaldehyde, Anal. Chim. Acta 625 (2008) 41–46.
[23] S. Goswami, S. Das, K. Aich, B. Pakhira, S. Panja, S.K. Mukherjee, S. Sarkar, A chemodosimeter for the ratiometric detection of hydrazine based on return of ESIPT and its application in live-cell imaging, Org. Lett. 15 (2011) 5412–5415.
[24] C. Hu, W. Sun, J. Cao, P. Gao, J. Wang, J. Fan, F. Song, S. Sun, X. Peng, A ratiometric near-infrared fluorescent probe for hydrazine and its in vivo applications, Org. Lett. 15 (2013) 4022–4025.
[25] L. Cui, Z. Peng, C. Ji, J. Huang, D. Huang, J. Ma, S. Zhang, X. Qian, Y. Xu, Hydrazine detection in the gas state and aqueous solution based on the Gabriel mechanism and its imaging in living cells, Chem. Commun. 50 (2014) 1485–1487.
[26] B. Chen, X. Sun, X. Li, H. Ågren, Y. Xie, Sens. Actuat. B 199 (2014) 93–100.
[27] B. Liu, Q. Liu, M. Shah, J. Wang, G. Zhang, Y. Pang, Sens. Actuat. B 202 (2014) 194–200.
[28] Y. Sun, D. Zhao, S. Fan, L. Duan, Sens. Actuat. B 208 (2015) 512–517.
[29] H.N. Kim, M.H. Lee, H.J. Kim, J.S. Kim, J.Y. Yoon, A new trend in rhodamine-based chemosensors: application of spirolactam ring-opening to sensing ions, Chem. Soc. Rev. 37 (2008) 1465–1472.
[30] A. Banerjee, A. Sahana, S. Lohar, I. Halui, S.K. Mukhopadhyay, D.A. Safin, M.G. Babashkina, M. Bolte, Y. Garcia, D. Das, A rhodamine derivative as a "lock" and SCN^- as a "key": visible light excitable SCN^- sensing in living cells, Chem. Commun. 49 (2013) 2527–2529.
[31] T.F. Slater, B. Sawyer, U. Sträuli, Studies on succinate-tetrazolium reductase systems. iii. points of coupling of four different tetrazolium salts, Biochim. Biophys. Acta 77 (1963) 383–393.
[32] T. Mosmann, Rapid colorimetric assay for cellular growth and survival: application to proliferation and cytotoxicity assays, J. Immunol. Methods 65 (1983) 55–63.
[33] M.V. Berridge, P.M. Herst, A.S. Tan, Tetrazolium dyes as tools in cell biology: new insights into their cellular reduction, Biotechnol. Annu. Rev. 11 (2005) 127–152.
[34] R.F. Kubin, A.N. Fletcher, Fluorescence quantum yields of some rhodamine dyes, J. Lumin 27 (1983) 455–462.
[35] E. Austin, M. Gouterman, Porphyrins. XXXVII. Absorption and emission of weak complexes with acids, bases, and salts, Bioinorg. Chem. 9 (1978) 281–298.
[36] V. Dyadkin, 2013.
[37] CrysAlisPro, Agilent Technologies, 2013.
[38] A.L. Spek, Structure validation in chemical crystallography, Acta Crystallogr. D. Biol. Crystallogr. 65 (2009) 148–155.
[39] M.C. Burla, R. Caliandro, B. Carrozzini, G.L. Cascarano, C. Giacovazzo, M. Mallamo, A. Mazzone, G. Polidori, http://wwwba.ic.cnr.it/content/sir2011-v10.
[40] G.M. Sheldrick, A short history of SHELX, Acta Crystallogr. A 64 (2008) 112–122.
[41] C.B. Hübschle, G.M. Sheldrick, B. Dittrich, ShelXle: a Qt graphical user interface for SHELXL, J. Appl. Crystallogr. 44 (2011) 1281–1284.
[42] I.J. Bruno, J.C. Cole, P.R. Edgington, M. Kessler, C.F. Macrae, P. McCabe, J. Pearson, R. Taylor, New software for searching the Cambridge structural database and visualizing crystal structures, Acta Crystallogr. B 58 (2002) 389–397.
[43] M. Zhu, M. Yuan, X. Liu, J. Xu, J. Lv, C. Huang, H. Liu, Y. Li, S. Wang, D. Zhu, Visible near-infrared chemosensor for mercury ion, Org. Lett. 10 (2008) 1481–1484.
[44] O. Gavet, J. Pines, Progressive activation of CyclinB1-Cdk1 coordinates entry to mitosis, Dev. Cell 18 (2010) 533–543.
[45] C.A. Schneider, W.S. Rasband, K.W. Eliceiri, NIH Image to ImageJ: 25 years of image analysis, Nat. Methods 9 (2012) 671–675.